ISSN: 0067-2904

Green Synthesized Titanium Dioxide Nanoparticles from date seed for photocatalytic dye degradation

Mohamed Abdelkalik Hussain*,Wadhah Naji Al Sieadi
Department of Chemistry, College of Science, University of Baghdad, Baghdad, Iraq

Received: 18/3/2024 Accepted: 17/10/2024 Published: 30/11/2025

Abstract

One of the most pressing challenges in the field of photocatalysis is the development of efficient photodegradation systems that utilize different ultraviolet light spectra and nanoparticles as photocatalysts to effectively remove pollutants from the environment. This study investigates the photodegradation efficiency of methylene blue dye under three different types of UV light sources using a new homemade instrument. The photodegradation activity of this system comprises various conditions, the first one is for MB dye only, the second one is when irradiation of MB dye with UV-A, UV-B, UV-C light sources with circulation, finally, the effect of adding 0.05 gm of green synthesis of TiO_2NPs by using date seed powder in sol-gel method. Different percentages of MB dye removal were reported. The prepared catalysts were characterized using Ultraviolet-visible spectroscopy, Fourier transform infrared spectroscopy, Scanning electron microscope, Energy dispersive analysis, X-ray spectroscopy, and atomic force microscopy. The photodegradation performance under UV-C irradiation was the highest, showing 98% photodegradation of MB dye in 90 minutes. UV-B irradiation showed 86% photodegradation of MB dye in 90 minutes, while UV-A irradiation showed 36% photodegradation of MB dye in 90 minutes.

Keywords: Green synthesis; TiO_2NPs; Date seed; Photodegradation; Sol-gel method.

التخليق الأخضر لجسيمات أوكسيد التيتانيوم النانوية باستخدام بذور النخيل وذلك للتحلل الضوئي للصبغة

محمد عبد الخالق حسين* ، وضاح ناجي السعيدي
قسم الكيمياء، كلية العلوم، جامعة بغداد، بغداد، العراق

الخلاصة

يُعد تطوير أنظمة تحلل ضوئي فعالة تستخدم أطياف الأشعة فوق البنفسجية المختلفة والجسيمات النانوية كمحفزات ضوئية لإزالة الملوثات من البيئة بشكل فعال أحد التحديات الأكثر إلحاحًا في مجال التحفيز الضوئي. تبحث هذه الدراسة في كفاءة التحلل الضوئي لصبغة الميثيلين الأزرق تحت ثلاثة أنواع مختلفة من مصادر الأشعة فوق البنفسجية باستخدام أداة جديدة محلية الصنع. تشتمل الدراسة تأثير التشعيع على صبغة الميثيلين الزرقاء، كذلك تأثير تشعيع صبغة الميثيلين الزرقاء عند إضافة (0.05) غم من جسيمات أوكسيد

*Email: muhamedabdelkalik@gmail.com

التيتانيوم النانوية والمخلقة بطريقة خضراء باستخدام مسحوق بذور التمر. توصلت الدراسة الى تحديد نسب مختلفة من تفكك صبغة المثيلين الزرقاء. تم استخدام تقنيات متنوعة لدراسة بُنية وسطح جسيمات أوكسيد التيتانيوم النانوية، حيود الاشعة السينية(XRD) ، المجهر الالكتروني الماسح مع التحليل الطيفي للأشعة السينية المشتتة للطاقة (FESEM–EDX) ومطياف الاشعة تحت الحمراء(FTIR)، مطيافية الاشعة فوق البنفسجية والمرئية (UV spectrophotometer)، المجهر الذري (AFM). بينت النتائج ان أداء التحلل الضوئي تحت إشعاع UV–C هو الأعلى، حيث أظهر تحللًا ضوئيًا بنسبة 98% لصبغة MB في 90 دقيقة. بينما أظهر إشعاع UV–B تحللًا ضوئيًا بنسبة 86% لصبغة MB في 90 دقيقة، بينما أظهر إشعاع UV–A تحللًا ضوئيًا بنسبة 36% لصبغة MB في 90 دقيقة.

1-Introduction

Nanotechnology has garnered significant attention in recent times. This field encompasses substances, materials, and devices that fall within the size range of 1 to 100 nanometers, a scale that has opened up new avenues for research and innovation [1]. Particles which have at least one dimension less than approximately 100 nanometers are known nanomaterials[2-3]. Although the particle size is what defines it as a nanomaterial, its geometry and morphology have a big effect on how it behaves[4]. With different sectors, the application of nanoparticles includes electronics, agriculture, biomedical, medicines, and environment[5-6].

Traditionally methods for synthesized nanoparticles, such as wet chemistry, frequently rely on the use of organic solvents, which are exceedingly used in these methods which involve nanomaterial synthesis[7-8]; additionally, the production of carbon dioxide in these methods which has a big concern with environment [9]. Overall, these techniques pose irreversible to the environment and scientists conducting synthesis, traditional nanomaterial methods have the potential to outweigh harms on synthesis benefits [10-11].
Natural sources such as plant extract, including leaves, seeds, and flowers [12-13] as well as microorganisms like yeasts[14], bacteria [15], and fungi [16]), contain bioactive agents, which are used in green synthesis of metal nanoparticles[17-18].
Plants in nature contain bioactive compounds, such as flavonoid[19], alkaloid[20], sugar[21], polyphenol[22], organic acid[23], terpenoid[24], antioxidant[23], and quinone, together with proteins which has low molecular weight[25]. These bioactive compounds act as reduction agents in the synthesis of nanomaterials procedures as electron donors or capping agents [26]. Through electrostatic interaction, these coating agents prevent intermediate products during the green synthesis process[27-28].

The seeds of the Iraqi date palm variety (Ashrasy) have been selected in this study; date fruit is commonly recognized. Date seeds contain bioactive compounds[30], such as fibre [31], carbohydrates[29], phenols[32], protein[33], and minerals (magnesium, potassium, phosphorus, iron, sodium, and calcium[34]).
These substances play biological roles, such as antibacterial, and antioxidant[35]. Date seeds are also a good source of oil (5 to 13%)[29], which makes date seeds promising candidates for deriving extracts in the synthesis of nanoparticles [32, 36]. It is suggested that during the synthesis process of nanoparticles, date seed extract played a role as a stabilizing and reducing agent [30, 37].

Photocatalysis using semiconductors for the degradation of organic pollutants does not require additional chemicals[38]. TiO_2NPs or titania known as semiconducting substances become a promising material with unique chemical, optical, and electronic properties[39], TiO_2NPs are known for non-toxicity, high chemical stability, high photocatalytic activity,

low cost, and environmental friendliness[40], exists commonly in three crystalline phases, rutile, brookite, anatase[41], the anatase phase has an effective photocatalytic activity of degrading organic pollutants of water[42]. One limitation of TiO_2NPs is their large band gap, which restricts their absorption to UV radiation, resulting in limited visible light absorption. To address this, TiO_2NPs can be doped with metals like gold, or coupled with semiconductors such as graphene[43]. In this work, photocatalytic activity was carried out using a new instrument design to irradiate the methylene blue by using UV irradiation UV-A, UV-B, and UV-C, by using TiO_2NPs which is obtained from green synthesis by the sol-gel method from the aqueous extract of date seed that improves the photocatalytic processes.

2.Materials and Methods

2.1 Chemicals and materials

Titanium tetrachloride ($TiCl_4$) (99.99%) with CAS, 7550-45-0, was supplied from Sigma Aldrich, America. Methylene blue dye ($C16H18ClN3S \cdot xH2O$), (≥95%), CAS, 61-73-4, was sourced from Merck, America. Ammonia (≥10%) CAS, 1336-21-6, bought from Prolabo, Canada. All experiments utilized deionized water.

2.2 Preparation of Date palm seed Aqueous:

Date palm seeds were purchased from the market, and the seeds were collected and washed with distilled water to remove any residual palm material. The seeds were then dried in an oven for 8 hours, after 24 hours, the seeds were ground to powder using a grinder from Al saif-elec, model HM-917, 220-240 V, 50/60Hz, 1200W, China. Ten grams of date seed powder (DSE) was added to 100ml DW, and then the mixture was heated using a stirrer hot plate type cimarec model MA-187, China, the temperature kept under 60 ^{0}C, mixture stirring at 180 rpm for 30 min, a brown solution was obtained, the mixture cooled down at room temperature, filtered, stored in a dark place for later used in green synthesis of TiO_2NPs.

2.3 Preparation of green TiO_2 NPs by the Sol-Gel:

To synthesize TiO_2NPs using the sol-gel method, 50 ml of 0.5M $TiCl_4$ was mixed with 50 ml of date seed juice. The mixture was heated to 60 ^{0}C with stirring, then, ammonia solution of 10 ml was added dropwise, and a yellow milky solution was obtained which was centrifuged to precipitate the sold. The next step was filtering and drying it in an oven with hot air for 24 hours, then using crystal mortar to grind the TiO_2NPs to powder. Finally, the yellowish TiO_2NPs were purified by calcination at a high temperature of 450 °C for 3-4 hours in a furnace to remove any absorbed moisture, resulting in a clear white powder, as shown in Figure 1. The TiO_2NPs was characterized by AFM, SEM, FTIR, UV-Vis spectrum, XRD, and EDAX.

Figure 1: TiO_2-NPs green synthesis steps by the Sol-Gel method.

2.4 Photoreactor and UV light sources:

A homemade photoreactor system was designed for this procedure, as shown in Figure 2. The system utilized a frame bought from the market, and a water diaphragm pump with 650-750mt rated flow 0.3A was attached to the frame. A UV lamp chamber, also acquired from the market and connected to the frame, to close the circle of flowing, a water cartridge with 10 inches where used, plastic tubes connected to a water purifier were used, the UV-light source used (T5 8W) UV-A (365 nm), (T5 8W) UV-B (311 nm), (T5 8W), UV-C (254 nm), all sourced from coospider Quartz Ultraviolet Lamp, 220v, China.

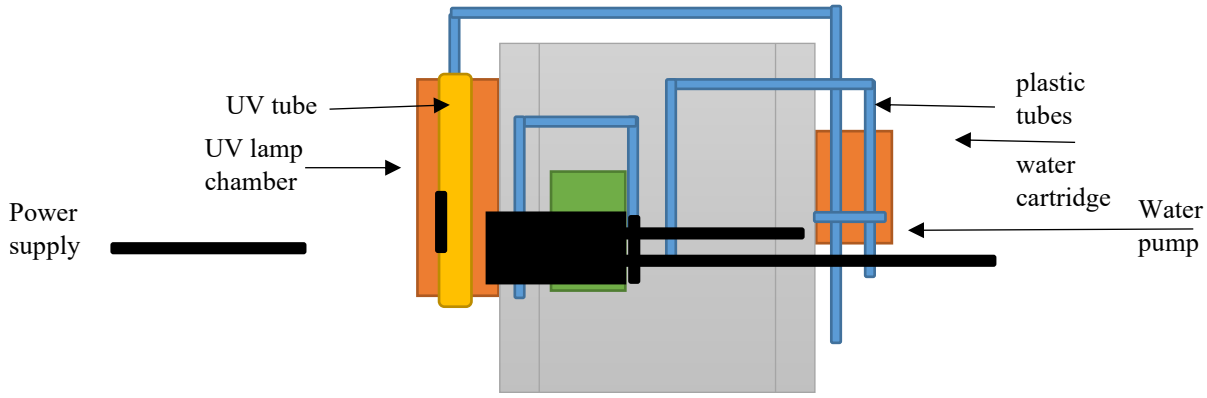

Figure 2: Homemade photoreactor system.

2.5 Photodegradation procedure:

The volume of solution required for the homemade photoreactor system has been measured (320ml) of MB dye with a concentration of ($6x10^{-6}$M, pH = 6.4). The first set of experiments was done to study the circulation effect on MB dye in the system without any irradiation or loading TiO_2NPs, second set of experiments was done to study the irradiation effect with UV-A, UV-B, and UV-C on MB dye without loading TiO_2NPs. The final set of experiments involved adding 0.05 g of TiO_2 NPs to the system to study the effect of TiO_2NPs with the irradiation of UV-A, UV-B, and UV-C on MB dye.

To achieve the adsorption-desorption equilibrium of MB dye on the surface of the photocatalyst, the solution was kept in a dark place for 15 minutes. Each experiment lasted 90 minutes, with a 2.5 mL sample collected from the system before the irradiation started, when irradiation started, the sample was collected every (15) minutes by using (1ml) pipette. All samples were centrifuged at 4000 rpm, prior to analysis with UV-VIS double beam spectrophotometer.

2.6. Photodegradation kinetic study:

The photocatalytic study of TiO_2NPs was examined, and the photodegradation rate of MB dye was calculated by using the following Eq. (1)[44], [45]:

$$\text{MB Degradation (\%)} = \frac{A0-At}{A0} \times 100 \quad (1)$$

Where A0 is the absorbance of initial MB; At is the absorbance of the solution after irradiation at time t. According to first-order kinetics reaction, rate constant k (min^{-1}) was determined by using the following relation Eq. (2)[46-47]:

$$\ln\left(\frac{Ct}{C0}\right) = -kt \quad (2)$$

where C0 and Ct are concentrations at the beginning and at a certain time, t is the irradiation time.

2.7. Characterization of Titanium oxide nanoparticles:

An X-ray diffractometer (XRD) from persee China model XD3, was utilized to identify the composition and structure of TiO_2NPs, operating conditions of 60 kV and 50 mA from range -40-90° at a scanning speed 0.125°-120°/ min, step size of 0.00025° with scanning radius 180mm. To measure the absorbances MB dye. A BOYN double-beam BNUV-D8000 UV−Vis spectrophotometer (China) was used. To identify the compounds' functional groups, FTIR analysis was performed using a Vertex-80v FTIR spectrometer connected to a Hyperion 3000 IR microscope (Bruker Optics GmbH, Germany), frequency range 4000–400 cm^{-1}. The mean diameters of TiO_2NPs and surface roughness are measured by atomic force microscopy (NaioAFM 2022 model, Nanosurf AG, Switzerland). Environmental scanning electron microscopy (ESEM) and Energy-dispersive X-ray spectroscopy (EDX) for elemental analysis were conducted using a Tescan Mira 3 (French) with resolution 1.2 nm at 30 kV; 2.3 nm at 3 kV.

3. Results and discussion

3.1. Morphological analysis

3.1.1 Scanning Electron Microscope and Energy Dispersive Analysis of X-ray:

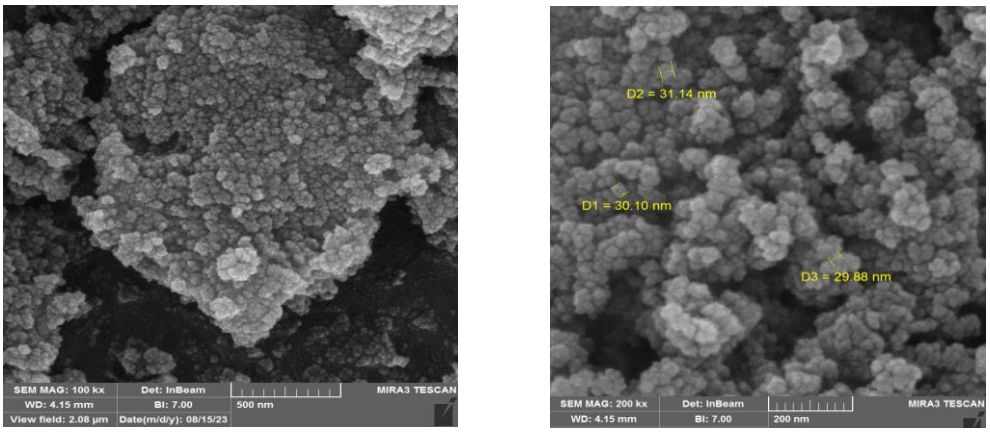

Figure 3: SEM images of TiO_2NPs view field (a) 2µm (b) 1µm.

The SEM analysis of green TiO_2NPs was conducted to examine the surface morphology, as shown in Figure 3. b. The synthesized TiO_2NPs exhibited a spherical shape with an average size of 30 nm, which indicates a high surface area of the prepared TiO_2NPs. Figure 3. a shows slight agglomerations, which is attributed to the high calcination temperature used to accelerate the crystal growth of TiO_2NPs.

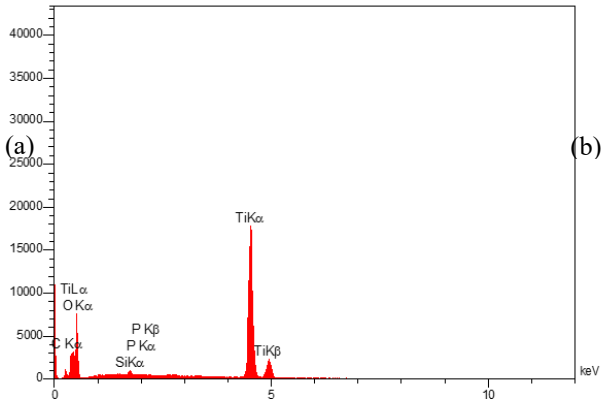

(a) (b)

Figure 4: EDAX spectrum (Energy dispersive analysis of X-ray) of green TiO_2NPs

Figure 4 presents the energy dispersive analysis of X-ray (EDAX) spectra for synthesized green TiO_2NPs, chemical composition and different elements in terms of weight percentage (Wt.%) and atomic percentage (At%) as shown in Table 1. The spectra reveal a prominent peak of titanium with high KeV, with high weight and atomic percentage, other elements are shown because of the effect of using date seed compounds in the syntheses of TiO_2NPs.

Table 1: Chemical composition of green TiO_2NPs in terms of weight and atomic percentage from (EDAX) measurement

Elements	Weight percentage (Wt. %)	Atomic percentage (At %)
C	3.10	5.79
O	51.14	71.79
Si	2.22	1.77
P	0.85	0.61
Ti	42.70	20.02
Total	100.00	100.00

3.1.2 X-ray diffraction (XRD):

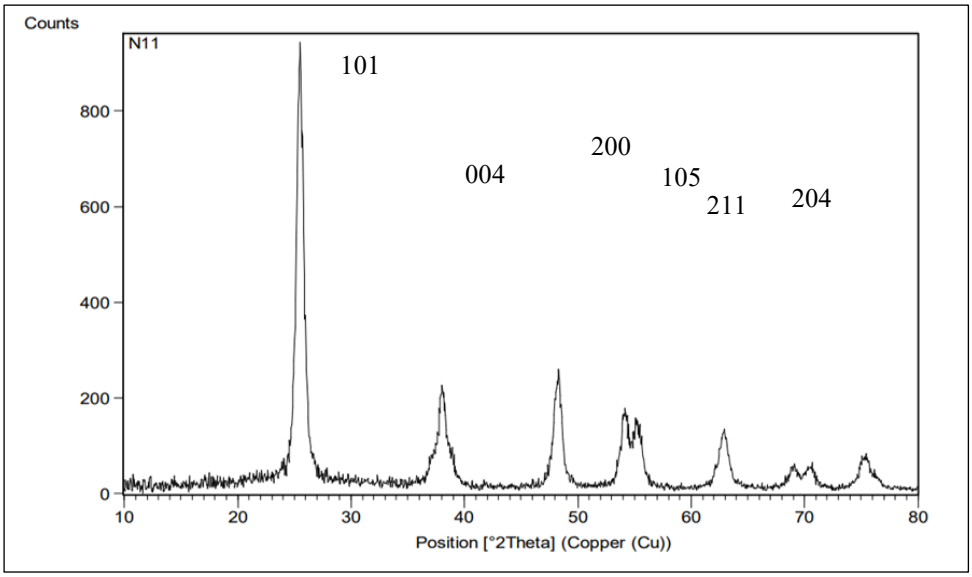

Figure -5: XRD pattern of green synthesis TiO_2NPs

The crystalline phase and structure of TiO_2NPs were analyzed using X-ray diffraction with a Cu-Kα diffractometer X-rays, (λ) 1.5406 Å, 2θ range of 0° to 80° step size of 0.00025°. The spectrum shows well defined, sharp peaks, indicating the crystalline of TiO_2NPs as it shown in Figure 5, the results identical with anatase phase patterns of TiO_2NPs from (JCPDS file 73-1764)[48], The diffraction peaks indeed appeared at 2θ = 25.5°, 37.11°, 47.5°, 54.2°, 55.13°, and 63.5°, confirming that the crystal planes are tetragonal. The average crystallite size for the anatase TiO_2NPs (101), (004), (200), (105), (211), and (204), respectively, which estimated according to the Debye−Scherrer's equation[49]:

$$D = \frac{K*\lambda}{\beta * \cos\theta} \quad (3)$$

Where D is NPs crystalline size, K represents the Scherrer constant (0.94), λ is the X-ray wavelength, β is the peak width at half maximum and θ is the Bragg's diffraction angle. The average particle size has been calculated to be (31.7 nm) as shown in Table 2.

Table 2: Average particle size calculation according to Debye−Scherrer's equation

k	λ	2 θ°	Cos θ°	β°	D	Average NPs
0.94	1.54	25.5	0.22252948	0.182142857	35.71485385	31.70354348
		37.11	0.323845843	0.142730769	31.31790063	
		47.5	0.414515697	0.11875	29.40857455	
		54.2	0.472984227	0.090333333	33.88081743	
		55.13	0.481100008	0.091883333	32.7473731	
		63.5	0.554142038	0.096212121	27.15174133	

3.1.3 FTIR spectroscopy study:

To identify the main functional groups, present in TiO_2NPs synthesised with date seed powder, an FTIR spectroscopy was employed for both date seed and green synthesized TiO_2NPs powder as shown in Figure 6 a, b. The absorption spectra, spanning the range of 4000–400 cm^{-1}, reveal several peaks indicative of high-purity product formation of TiO_2NPs. Peaks observed around 3425.34 cm^{-1} are attributed to O–H symmetric and asymmetric stretching vibrations of the hydroxyl groups (Ti-OH)[50].

Peaks around 1639.38 cm^{-1} are attributed to (C=O) stretching vibrations groups, peaks at 1564.16 cm^{-1} may represent C=N vibrations. The peaks observed at 1413.72 cm^{-1} can be attributed to the C-H bending [28–29]. For the pure TiO_2, it was reported the peaks at the broadband from 800 to 400 cm^{-1} region is attributed to the Ti-O stretching and Ti-O-Ti vibration absorption from the anatase TiO_2NPs[51-52].

3.1.4 Atomic force microscopy (AFM):

The topography of the TiO_2NPs phases was analyzed using AFM, which offer a large microstructural arrays surface inspection. Figure 7, show the (3D) image with for TiO_2NPs.

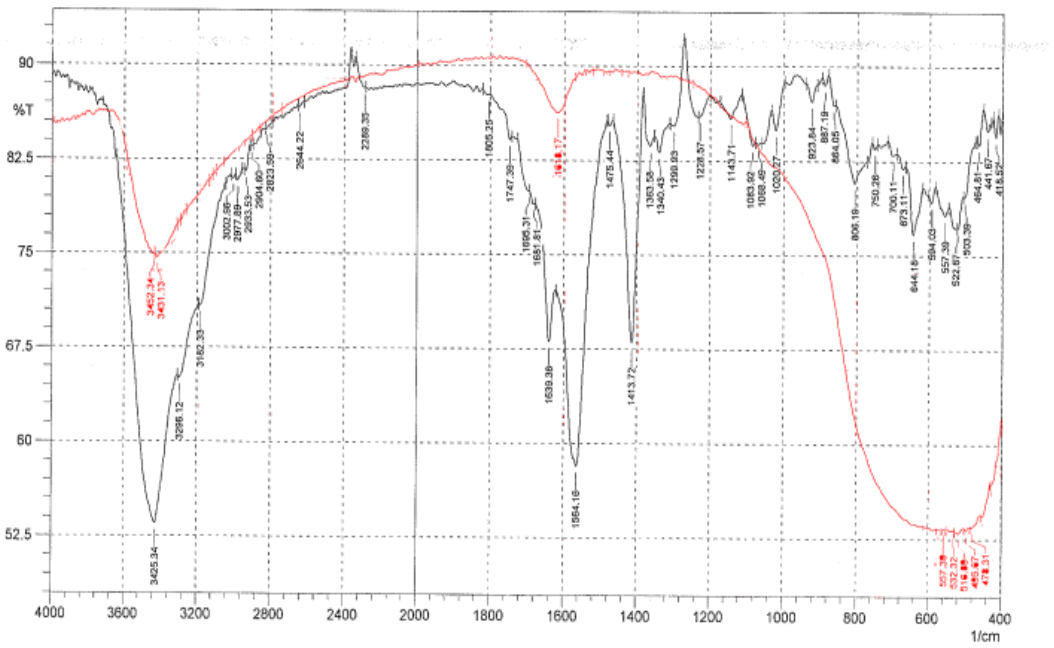

Figure 6: FTIR pattern of (a) Date seed (b) green synthesis TiO_2NPs

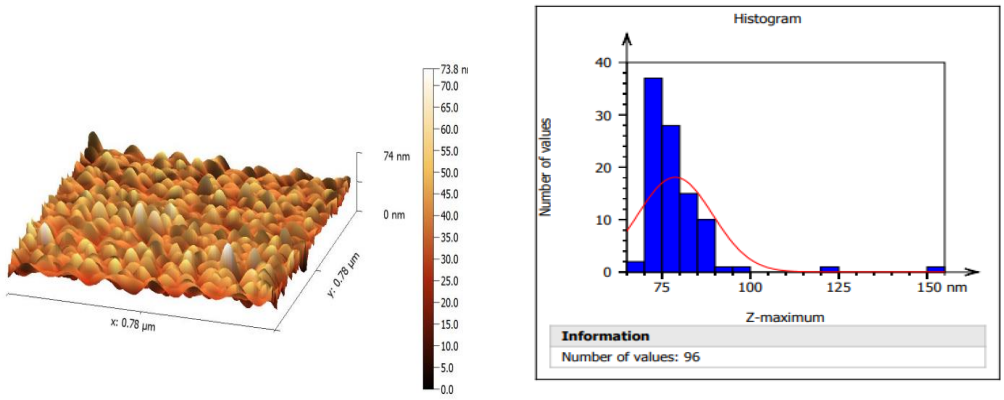

Figure 7: Atomic force microscopy analysis of TiO_2NPs

Table 3 presents the surface average roughness (surface area: 5.41456 µm2), and root mean square (RMS). It is noted that the anatase TiO_2NPs exhibit a small average median (35 nm), which can be observed anatase TiO_2NPs phase as one significant parameter.

Table 3: Average roughness, root mean square, average median for TiO_2NPs

Average value	Minimum	Maximum	Median	Rms (grain-wise)
35.50 nm	0.00 nm	76.39 nm	35.27 nm	5.92 nm

3.1.5 UV–Vis Spectroscopy of TiO2-NPs:

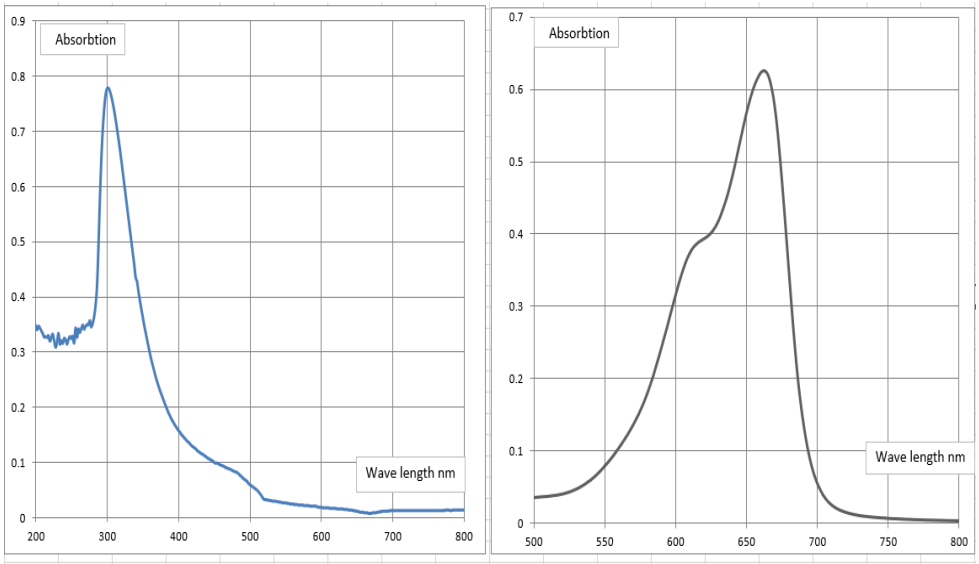

Figure 8: UV-Vis absorbance spectra (a) TiO_2NPs (b) Date seed

The absorbance edge spectra of TiO_2NPs are observed in the UV region at 300nm, while the DS spectra appear in the visible range at 662 nm, as shown in Figure 8, while the band gap obtained from the calculations made from TiO_2NPs UV absorbance spectra is 3.3 e.V as shown in Figure 9, which confirms the anatase TiO_2NPs[53-55].

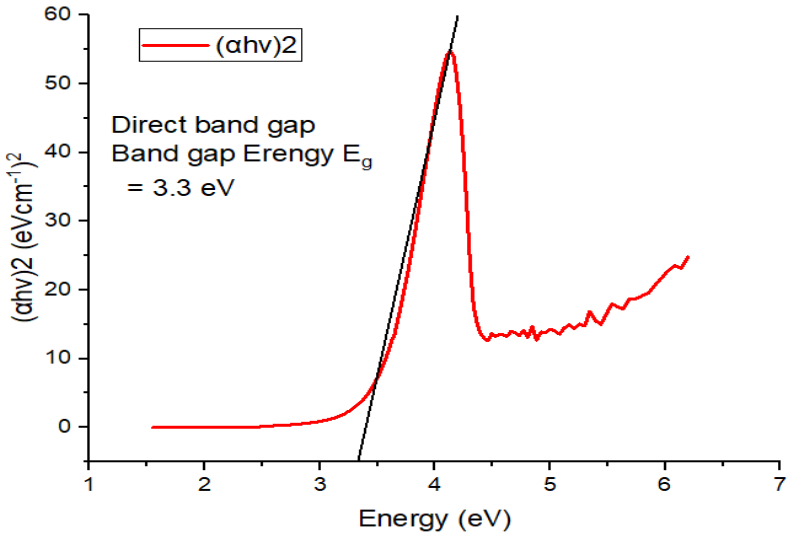

Figure 9: The band gap of green synthesis anatase TiO_2NPs

3.2. Photodegradation Studies

3.2.1 Absorption of TiO_2NPs:

The concentration selected for the experimental part was 20ppm (6×10^{-5}M) at 665nm wave length, with an absorbance of 0.680, as shown in Figure 10. According to Beer's law, this concentration of 20ppm lies between (0.2-0.7) absorbances with the least errors and best range for measurements[56].

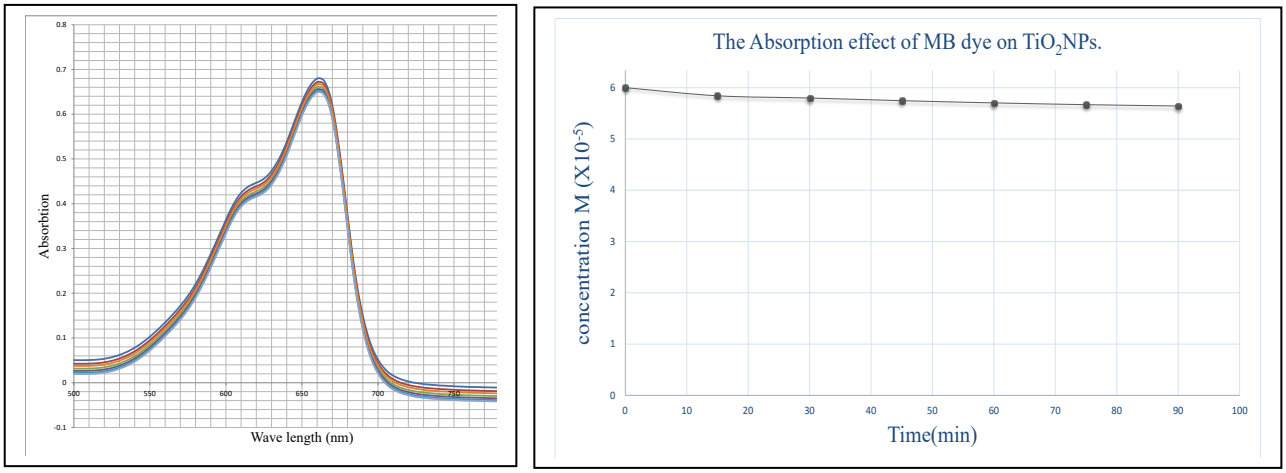

Figure 10: The adsorption effect on MB dye

3.2.2 Flow rate effect on degradation of MB dye:

The effect of flow rate on MB dye was investigated at a system flow rate of 750mlPM, MB absorbance and the relationship between the concentration and time which indicate a decrease in absorbance in (90) minute. The results showed degradation of MB in this experiment, the percentage was (14%) as illustrated in Figure 11.

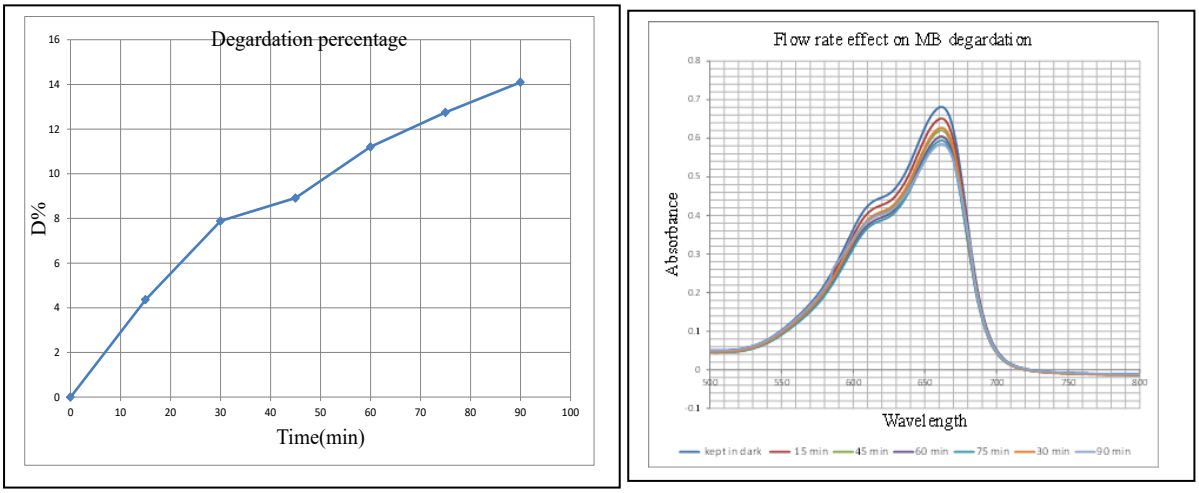

Figure 11: Degradation of MB dye in 90 minutes ([MB] = 20 ppm; TiO_2NPs loading = none)

3.2.3 Irradiation of MB dye with different UV-light sources:

The irradiation of MB with different lamps (UV-A, UV-B, UV-C) was conducted without the addition of a photocatalyst. All three experiments demonstrated a decrease in the MB concentration with time in different percentages, which indicates the photodegradation process with different percentages as shown in Figure. 12, The results show that photodegradation for UV-C = 34%, and both UV-B and UV-A results are 29% as shown in Figure 13.

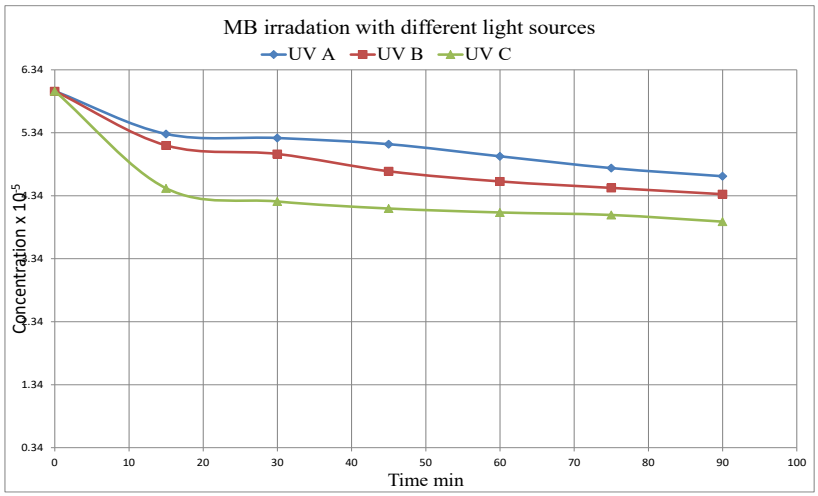

Figure 12: MB irradiation with different UV-light sources ([MB] = 20 ppm; TiO_2NPs loading = none)

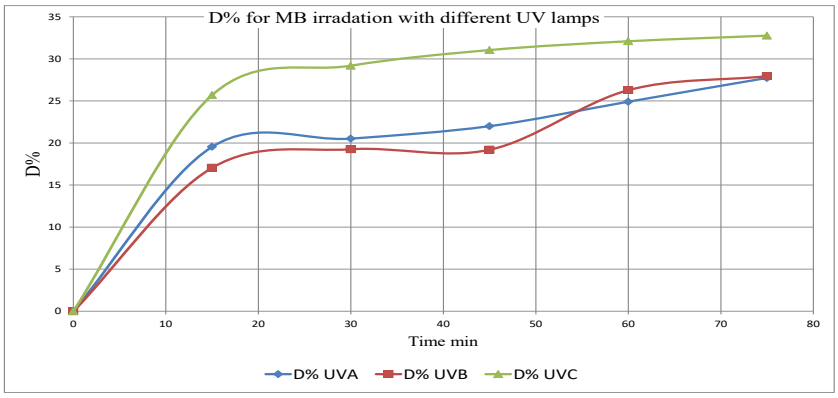

Figure 13: D% for MB irradiation with different UV lamps, ([MB] = 20 ppm; TiO_2NPs loading = none)

3.2.4 Methylene blue photodegradation with photocatalyst loading:

Figure 12 illustrates the photodegradation of MB with the addition of 0.05 g TiO_2NPs for 90 minute using different irradiation lamps in a new photoreactor system, lamps used are (UV-A (365 nm), UVB (311nm), UV-C (254 nm)). Figure 14 (a) shows MB decrease in concentration with time which indicates the photodegradation process with different percentages. Figures 14 (c) and (d) show the degradation percentage, with UV-C achieving 98% degradation, UV-B achieving 86% degradation, last UV-A achieving (36%) degradation. UV-C shows faster photodegradation of MB dye compared to UVB and UV-A, which indicates its capability roles in photolysis, as it has a shorter penetration wave length and high energy level.

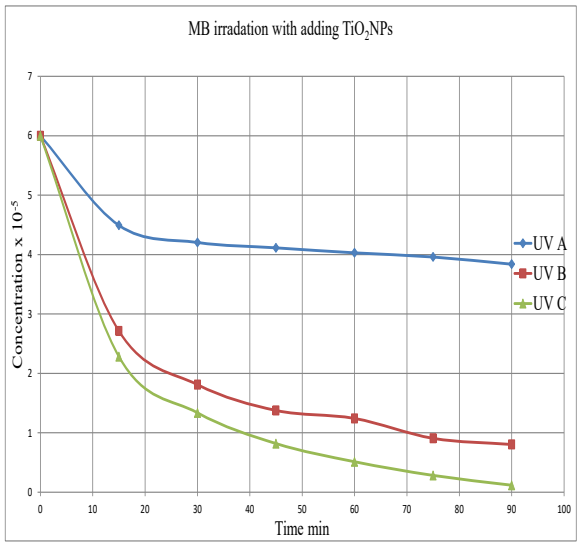

(a)

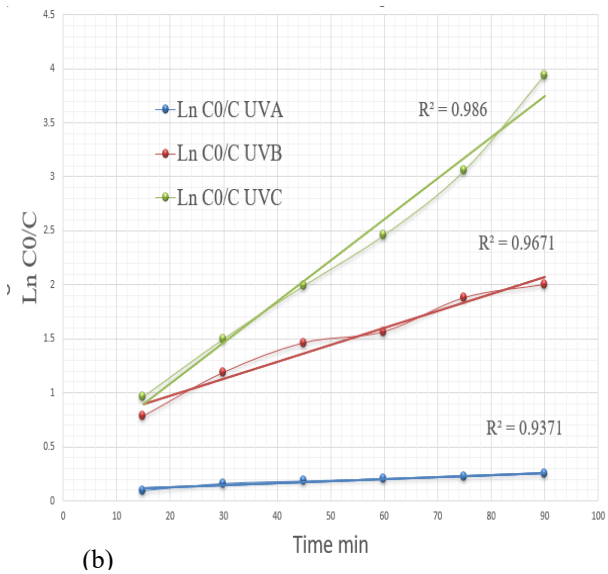

(b)

Figure 14: Photodegradation of MB (a) irradiation lamps effect UV-A, UV-B, UV-C on concentration, (b) Regression correlation values R^2, all experiments ([MB] = 20 ppm; TiO_2 NPs loading = 0.05g)

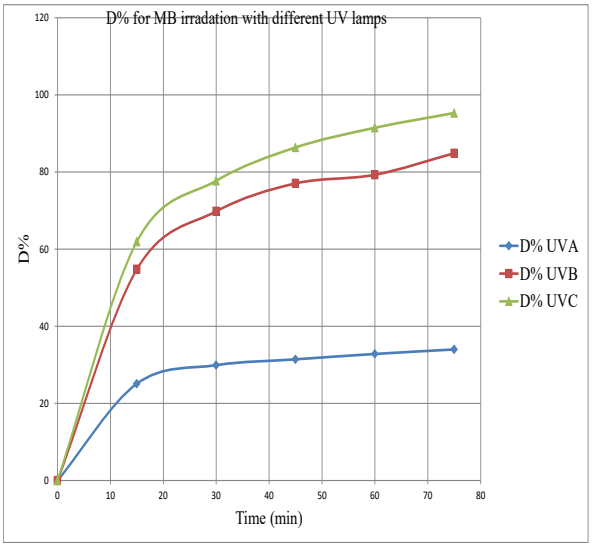

(c)

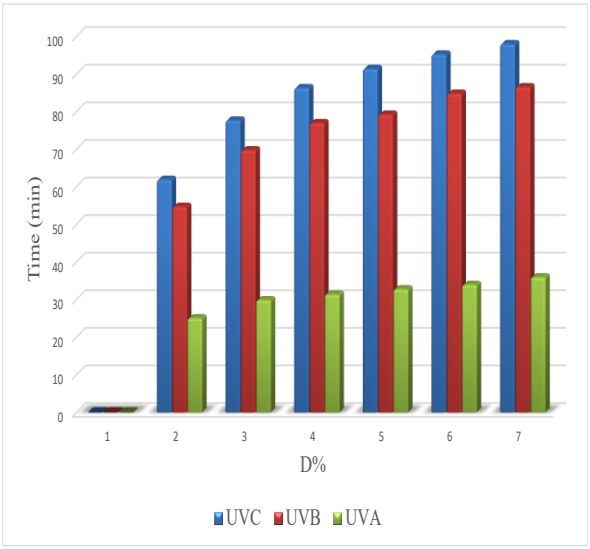

(d)

Figure 15: Photodegradation of MB (a) irradiation lamps effect UV-A, UV-B, UV-C (c) D% vs time, (d) D% chart with time.

The photodegradation study follows first order reaction kinetic [57-58]. A graph of ln(C0/Ct) against time was plotted as shown in Figure 14 (b), with high regression correlation value, all experiments fulfilled first order kinetics as shown in Table 4, UV-C showed the best regression correlation.

Table 4: Rate constant and regression correlation of different UV light sources

Experiment	Rate constant k(min^{-1})	Regression correlation R^2
UV-C	0.0644	0.9860
UV-B	0.0523	0.9671
UV-A	0.0064	0.9371

From Table 4, UV-C has the highest rate constant which indicates the high speed of reaction value (0.0644 min^{-1}), followed by UV-B (0.0523 min^{-1}), and UV-A (0.0064 min^{-1}), this parameter explains that the highest rate constant requires the least irradiation time to achieve complete degradation.

Conclusion

In this study, anatase TiO_2NPs were synthesized using a green synthesized method using date seed extract, the prepared nanoparticles are characterized to conform its morphology and surfaces. The new photoreactor which was designed and implemented for the photodegradation process achieved excellent results using different UV light sources UV-A, UV-B, and UV-C lamps, loading very small amount of TiO_2NPs can achieve 98% photodegradation of MB dye using-C lamp, 86% with UV-B lamp, last UV-A achieved 36%. The kinetics of photodegradation have been investigated, revealing that the reaction adheres to first-order kinetics. To illustrate this, a graph of ln(C0/Ct) versus time was constructed, which demonstrated a strong regression correlation (R^2) and enabled the determination of the rate constant for various UV light sources.

References

[1] R. Chandoliya, S. Sharma, V. Sharma, R. Joshi, and I. Sivanesan, "Titanium Dioxide Nanoparticle: A Comprehensive Review on Synthesis, Applications and Toxicity," *Plants*, vol.*13, no* 21, p.2964, Nov. 01, 2024.

[2] B. Mekuye and B. Abera, "Nanomaterials: An Overview of Synthesis, Classification, Characterization, and Applications," *Nano Select*, vol. 4, no. 8, pp. 486–501, 2023.
[3] R. Griffo, F. Di Natale, M. Minale, M. Sirignano, A. Parisi, and C. Carotenuto, "Analysis of Carbon Nanoparticle Coatings via Wettability," *Nanomaterials*, vol. 14, p. 301, 2024.
[4] T. Q. Tuan, L. Van Toan, and V. H. Pham, "Synthesis of Heterostructured TiO2 Nanopores/Nanotubes by Anodizing at High Voltages," *Materials*, vol. 17, no. 13, Jul. 2024.
[5] Z. Zhang, Y. Yang, and D. Cheng, "Fabrication of N-doped TiO2 Nanorods and Its Visible-Light Photocatalytic Activity for Resorcinol Degradation in Wastewater," *Int J Electrochem Sci*, vol. 16, pp. 1–12, 2021
[6] R. Alves Junior, H. P. A. Alves, J. M. Cartaxo, A. M. Rodrigues, G. A. Neves, and R. R. Menezes, "Use of nanostructured and modified TiO2 as a gas sensing agent,"Ceramica, vol. 67, p. 383, Jul. 01, 2021.
[7] M. A. Huq, M. Ashrafudoulla, M. M. Rahman, S. R. Balusamy, and S. Akter, "Green Synthesis and Potential Antibacterial Applications of Bioactive Silver Nanoparticles: A Review," *Polymers*, vol. 14, no. 4, p. 742, 2022.
[8] S. Saravanan, M. Balamurugan, and T. Soga, "Synthesis of Titanium Dioxide Nanoparticles with Desired Ratio of Anatase and Rutile Phases and the Effect of High Temperature Annealing," *Transactions of the Materials Research Society of Japan*, vol. 43, no. 5, pp. 255–261, Oct. 2018.
[9] W. Herrera, J. Vera, E. Hermosilla, M. Diaz, G. R. Tortella, R. A. D. Reis, A. B. Seabra, M. C. Diez, and O. Rubilar, "The Catalytic Role of Superparamagnetic Iron Oxide Nanoparticles as a Support Material for TiO2 and ZnO on Chlorpyrifos Photodegradation in an Aqueous Solution," *Nanomaterials*, vol. 14, no. 3, p. 299, 2024.
[10] H. G. Hameed and N. A. Abdulrahman, "Synthesis of TiO2 Nanoparticles by Hydrothermal Method and Characterization of their Antibacterial Activity: Investigation of the Impact of Magnetism on the Photocatalytic Properties of the Nanoparticles," *Physical Chemistry Research*, vol. 11, no. 4, pp. 771–782, 2023.
[11] M. Mujahid and O. A. Al-Hartomy, "The Effects of Pt-Doped TiO2 Nanoparticles and Thickness of Semiconducting Layers at Photoanode in the Improved Performance of Dye-Sensitized Solar Cells," *Materials*, vol. 15, no. 22, Nov. 2022.
[12] S. S. Bahria, Z. Haruna, S. K. Hubadillah, W. N. Salleh, N. Rosman, N. H. Kamaruddin, F. H. Azhar, N. Sazali, R. A. Ahmad, and H. Basri, "Review on Recent Advance Biosynthesis of TiO2 Nanoparticles from Plant-Mediated Materials: Characterization, Mechanism and Application," *IOP Conference Series: Materials Science and Engineering*, vol. 1142, no. 1, p. 012005, 2021.
[13] P. Sathishkumar, F. L. Gu, Q. Zhan, T. Palvannan, and A. R. Mohd Yusoff, "Flavonoids Mediated Green Nanomaterials: A Novel Nanomedicine System to Treat Various Diseases – Current Trends and Future Perspective," *Materials Letters*, vol. 210, pp. 26–30, 2018.
[14] V. Tadioto, A. Giehl, R. D. Cadamuro, I. Z. Guterres, A. A. Santos, S. K. Bressan, L. Werlang, B. U. Stambuk, G. Fongaro, I. T. Silva, and S. L. Alves, "Bioactive Compounds from and Against Yeasts in the One Health Context: A Comprehensive Review," *Frontiers in Microbiology*, vol. 9, no. 4, p. 363, 2023.
[15] Y. Xie, Q. Peng, Y. Ji, A. L. Yang, S. Mu, Z. Li, T. He, Y. Xiao, J. Zhao, and Q. Zhang, "Isolation and Identification of Antibacterial Bioactive Compounds from Bacillus Megaterium L2," *Frontiers in Microbiology*, vol. 12, p. 645484, 2021.
[16] N. Rousta, M. Aslan, M. Yesilcimen Akbas, F. Ozcan, T. Sar, and M. J. Taherzadeh, "Effects of Fungal-Based Bioactive Compounds on Human Health: A Review," *Biomass Conversion and Biorefinery*, vol. 64, no. 20, pp. 7004–7027, 2023.
[17] Z. Zahra, Z. Habib, S. Chung, and M. A. Badshah, "Exposure Route of TiO2 NPs from Industrial Applications to Wastewater Treatment and Their Impacts on the Agro-environment," *Nanomaterials*, vol. 10, no. 8, p. 1469, 2020.
[18] A. K. Abass, W. N. J. Al Sieadi, and A. K. M. A. Al-Sammarraie, "Investigation of the Electrical, Compositional, and Magnetic Features of Hybrid Lead Oxide Nanocomposites," *Eurasian Chemical Communications*, vol. 4, no. 11, pp. 1044–1053, 2022.

[19] I. Dincheva, I. Badjakov, and B. Galunska, "New Insights into the Research of Bioactive Compounds from Plant Origins with Nutraceutical and Pharmaceutical Potential," *Plants*, vol. 12, no. 2, p. 258, 2023.

[20] M. Loi, C. Paciolla, A. F. Logrieco, and G. Mulè, "Plant Bioactive Compounds in Pre- and Postharvest Management for Aflatoxins Reduction," *Frontiers Media S.A.*, vol. 12, no. 11, p. 243, 2020.

[21] A. Tsakni, A. Chatzilazarou, E. Tsakali, A. G. Tsantes, J. Van Impe, and D. Houhoula, "Identification of Bioactive Compounds in Plant Extracts of Greek Flora and Their Antimicrobial and Antioxidant Activity," *Separations*, vol. 10, no. 7, p. 373, 2023.

[22] F. Fotsing Yannick Stéphane, B. Kezetas Jean Jules, G. El-Saber Batiha, I. Ali, and L. Ndjakou Bruno, "Extraction of Bioactive Compounds from Medicinal Plants and Herbs," in *Natural Medicinal Plants*, IntechOpen, vol. 10, no. 2, p. 5772, 2022.

[23] S. Albukhaty, L. Al-Bayati, H. Al-Karagoly, and S. Al-Musawi, "Preparation and Characterization of Titanium Dioxide Nanoparticles and In Vitro Investigation of Their Cytotoxicity and Antibacterial Activity Against Staphylococcus Aureus and Escherichia Coli," *Animal Biotechnology*, vol. 33, no. 5, pp. 864–870, 2022.

[24] H. M. Saleh and A. I. Hassan, "Synthesis and Characterization of Nanomaterials for Application in Cost-Effective Electrochemical Devices," *Sustainability*, vol. 15, no. 14, p. 10891, Jul. 01, 2023..

[25] J. A. S. Salman, A. A. Kadhim, and A. J. Haider, "Biosynthesis, Characterization and Antibacterial Effect of ZnO Nanoparticles Synthesized by Lactobacillus Spp," *Journal of Global Pharma Technology*, vol. 10, no. 03, pp. 348–355, 2018.

[26] B. M. Alghamdi *et al.*, "Regulating the Electron Depletion Layer of Au/V2O5/Ag Thin Film Sensor for Breath Acetone as Potential Volatile Biomarker," *Nanomaterials*, vol. 13, no. 8, Apr. 2023.

[27] A. Kadim, Z. Zainal, A. Mebdir, H. Lim, Z. Abidin, and Y. Lim, "Sensitization of TiO2 nanotube arrays photoelectrode via homogeneous distribution of CdSe nanoparticles by electrodeposition techniques," *The Journal of Physical Chemistry*, vol. 153, no. 2, p. 110006, 2021.

[28] M. T. Mohammed, W. N. Al-Sieadi, and O. H. R. Al-Jeilawi, "Characterization and synthesis of some new Schiff bases and their potential applications," *Eurasian Chemical Communications*, vol. 4, no. 6, pp. 481–494, 2022.

[29] A. Kadim, A. Ayat, K. Hashim, A. Mudhafar, M. Ahlam, and M. Farhan, "Electrochemical deposition of Cu nanoparticle loaded CdSe/TiO2 nanotube nanostructure as photoelectrode," *Journal of Electronic Materials*, vol. 50, no. 9, pp. 5161-5167, 2021.

[30] A. K. Ayal, "Effect of anodization duration in the TiO2 nanotubes formation on Ti foil and photoelectrochemical properties of TiO2 nanotubes," *Al-Mustansiriyah Journal Science*, vol. 29, no. 3, pp. 77-81, 2018.

[31] A. M. Holi, G. A. Al-Sajad, A. A. Al-Zahrani, and A. S. Najm, "Enhancement in NO2 and H2-sensing performance of CuxO/TiO2 nanotubes arrays sensors prepared by electrodeposition synthesis," *Nano Biomed Engineering*, vol. 14, no. 2, pp. 7-14, 2022.

[32] M. Ranasinghe, I. Manikas, S. Maqsood, and C. Stathopoulos, "Date components as promising plant-based materials to be incorporated into baked goods—A review," *Plants*, vol. 14, no. 2, p. 605, 2022.

[33] M. Kehili, A. Isci, N. Thieme, M. Kaltschmitt, C. Zetzl, and I. Smirnova, "Microwave-assisted deep eutectic solvent extraction of phenolics from defatted date seeds and its effect on solubilization of carbohydrates," *Biomass Conversion and Biorefinery*, vol. 14, no. 6, pp. 7695-7706, 2022.

[34] N. Dabetić, V. Todorović, M. Panić, I. R. Redovniković, and S. Šobajić, "Impact of deep eutectic solvents on extraction of polyphenols from grape seeds and skin," *Applied Sciences (Switzerland)*, vol. 10, no. 14, p. 4830, 2020.

[35] J. Osamede Airouyuwa, H. Mostafa, A. Riaz, and S. Maqsood, "Utilization of natural deep eutectic solvents and ultrasound-assisted extraction as green extraction technique for the recovery of bioactive compounds from date palm (Phoenix dactylifera L.) seeds: An investigation into optimization of process parameters," *Ultrasonics Sonochemistry*, vol. 91, p. 233, 2022.

[36] S. Bhattacharjee, F. Habib, N. Darwish, and A. Shanableh, "Iron sulfide nanoparticles prepared using date seed extract: Green synthesis, characterization and potential application for removal of ciprofloxacin and chromium," *Powder Technology*, vol. 380, pp. 219–228, 2021.

[37] J. Noh, S. H. Kwon, S. Park, K. K. Kim, and Y. J. Yoon, "Tio2 nanorods and pt nanoparticles under a uv-led for an no2 gas sensor at room temperature," *Sensors*, vol. 21, no. 5, pp. 1–11, Mar. 2021.

[38] M. M. Masood and W. N. Al-Sieadi, "Green synthesis of nickel oxide nanoparticles via *Imperata cylindrica* extract for dual application in photocatalytic degradation of rhodamine B dye and antibacterial activity," *Russian Journal of General Chemistry*, vol. 94, pp. 1727-1737, 2024.

[39] H. M. El Sharkawy, A. M. Shawky, R. Elshypany, and H. Selim, "Efficient photocatalytic degradation of organic pollutants over TiO2 nanoparticles modified with nitrogen and MoS2 under visible light irradiation," *Scientific Reports*, vol. 13, no. 1, pp. 45-67, 2023.

[40] M. Ghosh, P. Chowdhury, and A. K. Ray, "Photocatalytic activity of aeroxide TiO2 sensitized by natural dye extracted from mangosteen peel," *Catalysts*, vol. 10, no. 8, p. 917, 2020.

[41] M. Mollavali, S. Rohani, and M. Elahifard, "Band gap reduction of (Mo + N) co-doped TiO2 nanotube arrays with a significant enhancement in visible light photo-conversion: A combination of experimental and theoretical study," *International Journal of Hydrogen Energy*, vol. 46, no. 41, pp. 21475–21498, 2021.

[42] A. Farzaneh, M. Javidani, M. D. Esrafili, and O. Mermer, "Optical and photocatalytic characteristics of Al and Cu doped TiO2: Experimental assessments and DFT calculations," *Journal of Physics and Chemistry of Solids*, vol. 161, p. 110404, 2022.

[43] E. Y. Ahn, S. W. Shin, K. Kim, and Y. Park, "Facile green synthesis of titanium dioxide nanoparticles by upcycling mangosteen (Garcinia mangostana) pericarp extract," *Nanoscale Research Letters*, vol. 17, no. 1, p. 40, 2022.

[44] S. Alkaykh, A. Mbarek, and E. E. Ali-Shattle, "Photocatalytic degradation of methylene blue dye in aqueous solution by MnTiO3 nanoparticles under sunlight irradiation," *Heliyon*, vol. 6, no. 4, p. 3663, 2020.

[45] G. V. Geetha, R. Sivakumar, C. Sanjeeviraja, and V. Ganesh, "Photocatalytic degradation of methylene blue dye using ZnWO4 catalyst prepared by a simple co-precipitation technique," *Journal of Sol-Gel Science and Technology*, vol. 97, no. 3, pp. 572–580, 2021.

[46] T. Nakayama, R. Honda, K. Kuwata, S. Usui, and B. Uno, "Electrochemical and mechanistic study of reactivities of α-, β-, γ-, and δ-tocopherol toward electrogenerated superoxide in N,N-dimethylformamide through proton-coupled electron transfer," *Antioxidants*, vol. 11, no. 1, p. 9, 2022.

[47] J. Iqbal, B. A. Abbasi, T. Yaseen, S. A. Zahra, A. Shahbaz, S. A. Shah, S. Uddin, X. Ma, B. Raouf, S. Kanwal, W. Amin, T. Mahmood, H. A. El-Serehy, and P. Ahmad, "Green synthesis of zinc oxide nanoparticles using Elaeagnus angustifolia L. leaf extracts and their multiple in vitro biological applications," *Scientific Reports*, vol. 11, no. 1, p. 20988, 2021.

[48] M. Kouchakzadeh, A. Honarbakhsh, S. M. Movahedifar, R. Zhiani, and F. Hajian, "Photocatalysts under visible-UV light for removal of organic dyes using dendritic fibrous nano-titanium modified with DyVO4 nanoceramic," *Results in Chemistry*, vol. 6, p. 101136, 2023.

[49] R. Ahmadiasl, G. Moussavi, S. Shekoohiyan, and F. Razavian, "Synthesis of Cu-doped TiO2 nanocatalyst for the enhanced photocatalytic degradation and mineralization of gabapentin under UVA/LED irradiation: Characterization and photocatalytic activity," *Catalysts*, vol. 12, no. 11, 2022.

[50] X. Li, Y. Gao, H. Xiong, and Z. Yang, "The electrochemical redox mechanism and antioxidant activity of polyphenolic compounds based on inlaid multi-walled carbon nanotubes-modified graphite electrode," *Open Chemistry*, vol. 19, no. 1, pp. 961–973, 2021.

[51] A. Seifi, D. Salari, A. Khataee, B. Çoşut, L. Çolakerol Arslan, and A. Niaei, "Enhanced photocatalytic activity of highly transparent superhydrophilic doped TiO2 thin films for improving the self-cleaning property of solar panel covers," *Ceramics International*, vol. 49, no. 2, pp. 1678-1689, 2023.

[52] K. E. Al Ani, A. E. Ramadhan, and W. N. Al Sieadi, "Fourier-transform infrared spectroscopic study of plasticization effects on the photodegradation of poly(fluorostyrene) isomers films," *Journal of Vinyl and Additive Technology*, vol. 24, no. 1, pp. 75–83, 2018.

[53] S. M. Mustafa, A. A. Barzinjy, A. H. Hamad, and S. M. Hamad, "Green synthesis of Ni-doped ZnO nanoparticles using dandelion leaf extract and its solar cell applications," *Ceramics International*, vol. 12, pp. 29257-29266, 2022.

[54] A. Safeen, K. Safeen, R. Ullah, W. H. Shah, Q. Zaman, K. Althubeiti, S. Al Otaibi, N. Rahman, S. Iqbal, A. Khan, A. Khan, and R. Khan, "Enhancing the physical properties and photocatalytic activity of TiO2 nanoparticles via cobalt doping," *RSC Advances*, vol. 12, no. 25, pp. 15767–15774, 2022.

[55] A. K. Ayal, "Effect of anodization duration in the TiO2 nanotubes formation on Ti foil and photoelectrochemical properties of TiO2 nanotubes," *Al-Mustansiriyah Journal Science*, vol. 29, no. 3, pp. 77-81, 2018.

[56] W. B. Baker, A. B. Parthasarathy, D. R. Busch, R. C. Mesquita, J. H. Greenberg, and A. G. Yodh, "Modified Beer-Lambert law for blood flow," *Biomedical Optics Express*, vol. 5, no. 11, p. 4053, 2014.

[57] A. S. Rini, Y. Rati, R. Dewi, and S. Putri, "Investigating the influence of precursor concentration on the photodegradation of methylene blue using biosynthesized ZnO from Pometia pinnata leaf extracts," *Baghdad Science Journal*, vol. 20, pp. 2532–2539, 2023.

[58] S. A. Mousa, S. Tareq, and E. A. Muhammed, "Studying the photodegradation of Congo red dye from aqueous solutions using bimetallic Au-Pd/TiO2 photocatalyst," *Baghdad Science Journal*, vol. 18, no. 4, pp. 1261–1268, 2021.